A STATISTICAL FRAMEWORK FOR MATERIAL DECOMPOSITION USING MULTI-ENERGY PHOTON COUNTING X-RAY DETECTOR

Jiyoung Choi[1], *Dong-Goo Kang*[2], *Sunghoon Kang*[2], *Younghun Sung*[2], *and Jong Chul Ye*[1*]

[1]Bio-Imaging & Signal Processing Lab., Dept. Bio& Brain Engineering,
Korea Advanced Institute of Science & Technology (KAIST),
291 Daehak-ro, Yuseong-gu, Daejon 305-701, Republic of Korea
[2] Samsung Advanced Institute of Technology, Samsung Electronics
14-1, Nong-seo dong, Kiheung-gu, Yongin, Kyunggi, Republic of Korea
*jong.ye@kaist.ac.kr

ABSTRACT

Recently, material decomposition using multi energy photon counting x-ray detector (PCXD) have been one of the very active areas of researches. Even with a few success, decomposition of three materials, including malignant tissue, has been still considered a difficult problem and systematic studies are still required. In this paper, we propose a statistical framework for decomposition of three material using PCXD. In particular, we derive an energy level optimization algorithm using the theory of minimum variance unbiased estimator (MVUE), and iterative update of material composition as well as system parameter estimation under a unified statistical estimation framework. Experiment results using physical breast phantom as well as real *ex vivo* breast data confirm that the proposed algorithm can accurately decompose three materials including malignant tissue.

Index Terms— PCXD, material decomposition, statistical framework

1. INTRODUCTION

Breast cancer is one of the most common cancer in women. However, it has over 98% 5-year survival with early diagnosis. The detection of malignant tissues, such as calcification or carcinoma, is therefore important in early diagnosis of breast cancer. To distinguish malignant tissues from physiological structure of normal breast, material decomposition approach has been studied. In particular, injected contrast media has been exploited to detect breast cancer by exploiting high energy consumption of cancer. However, injection of contrast media can cause patient inconvenience and motion artifact due to the multiple measurements of pre- and post-injection.

Recently, material decomposition using multi-energy x-ray sources or detectors has been demonstrated without contrast media. Laidevant et al. decomposed mammography image into water, lipid, and protein [1] from dual energy measurements, based on previously suggested inverse mapping method [2] with known total object thickness. However, their method requires at least 20 calibration blocks to avoid over-fitting. Although Ducote and Molloi have accurately estimated glandular and adipose ratio of breast, [3], however, the estimated ratio does not directly indicate malignant tissue. Furthermore, systematic study of optimal energy or compensation for hardware imperfectness was not discussed in the previous studies.

In this research, we aim to decompose three materials including carcinoma using energy resolving PCXD in mammography environment. Unlike the conventional approaches [1, 2], we formulate the material decomposition problem in a statistical estimation framework based on the assumption that the PCXD measurement follows the Poisson statistics. The main advantage of this framework is that the optimal energy selection problem, system calibration problem as well as material decomposition problem can be formulated using a unified estimation framework. More specifically, we show that the optimal estimator for the material decomposition takes the form of the minimum variance unbiased estimator (MVUE), whose estimator error variance is minimum among all unbiased estimator. This implies that the energy optimization problem can be formulated as minimizing the trace of the resulting minimum covariance matrix. Furthermore, using calibration phantoms, system imperfectness correction can be performed as an attenuation coefficient estimation problem. Under the optimized energy level and attenuation coefficient parameters, the final material decomposition problem can be solved using a convex optimization problem with positivity constraint.

In both of physical phantom and *ex vivo* data, our algorithm accurately decomposed three materials including malignant tissue with optimized energy level measurements using fewer calibration blocks. In particular, in *ex vivo* data, the decomposed malignant tissue region is well matched to ground truth that a doctor marked.

2. A STATISTICAL FRAMEWORK OF MATERIAL DECOMPOSITION

2.1. Measurement model

Energy discriminating PCXD simultaneously acquires multi energy measurements by counting the number of photons corresponding to each energy bin, in contrast to conventional photon integrating detectors which measures all signals during time interval. Due to the energy discrimination threshold, electronic noise is effectively removed in PCXD. Therefore, we can assume Poisson distribution for detector measurement.

Since each energy bin of PCXD independently counts the number of photons, the probability density function (pdf) of measure-

This work was in part supported by Samsung Advanced Institute of Technology, Samsung Electronics, Republic of Korea, and in part by the Korea Science and Engineering Foundation (KOSEF) grant funded by the Korea government (MEST) (No.2011-0000353).

ment $\mathbf{d} = [d_1, \cdots, d_M]^T$ is

$$f(\mathbf{d}|\mathbf{t}) \quad = \quad \prod_{i=1}^{M} \frac{\lambda_i}{d_i!} \exp\left(-\lambda_i\right), \tag{1}$$

where λ_i is the expected mean and variance of i-th energy bin. For further simplification, the inverse log of normalized intensity can be approximated to linear combination of attenuation coefficients of bases materials [1], as $-\log \lambda_i \approx \mathbf{A}^i\mathbf{t} + b_i$ where $\mathbf{A}^i$ is the i-th row of $\mathbf{A}$ matrix, representing the effective attenuation coefficients of bases materials for i-th energy bin, and b_i refers the offset for linear approximation of polychromatic measurement which is originally nonlinear, while $\mathbf{t}$ refers the thickness of bases materials. With this approximation, the log-likelihood can be rewritten in the form of weighted l_2-norm for $\mathbf{t}$ as

$$L(\mathbf{t}|\mathbf{d}) \approx -\frac{1}{2}(\mathbf{y} - \mathbf{A}\mathbf{t} - \mathbf{b})^T\mathbf{\Lambda}(\mathbf{y} - \mathbf{A}\mathbf{t} - \mathbf{b}) + c(\mathbf{d}) \tag{2}$$

where $y_i = -\log\left(d_i/\bar{I}_i\right)$, $\mathbf{\Lambda} = diag(\mathbf{d})$, $c(\mathbf{d})$ is a function of $\mathbf{d}$, and $\bar{I}_i$ is the the nominal number of photons corresponding to i-th energy bin.

2.2. Energy level optimization

With log-likelihood approximation (2), the approximated pdf $f(\mathbf{d}|\mathbf{t}) = \exp(L(\mathbf{t}|\mathbf{d}))$ is in the form of multivariate Gaussian distribution about random variable $\mathbf{y}$ with covariance matrix $\mathbf{\Lambda}^{-1}$. Furthermore, this pdf can be divided into $f(\mathbf{d}|\mathbf{t}) \propto h(\mathbf{d})g(T(\mathbf{d})|\mathbf{t})$ where

$$h(\mathbf{d}) = \exp\left(-\frac{1}{2}(\mathbf{y} - \mathbf{b})^T\mathbf{\Lambda}(\mathbf{y} - \mathbf{b}) + c(\mathbf{d})\right)$$

$$g(T(\mathbf{d})|\mathbf{t}) = \exp\left(-\frac{1}{2}(\mathbf{A}\mathbf{t})^T\mathbf{\Lambda}(\mathbf{A}\mathbf{t})\right)\exp\left((\mathbf{A}\mathbf{t})^T\mathbf{\Lambda}(\mathbf{y} - \mathbf{b})\right).$$

Therefore, by the factorization theorem [4], the sufficient statistics $T(\mathbf{d})$ about $\mathbf{t}$ can be defined as

$$T(\mathbf{d}) = (\mathbf{A}\mathbf{t})^T\mathbf{\Lambda}(\mathbf{y} - \mathbf{b})\,. \tag{3}$$

Note that $T(\mathbf{d})$ is a complete sufficient statistics since pdf $f(\mathbf{d}|\mathbf{t})$ is a family of Gaussian distribution, which is well known as a complete distribution family.

By maximizing the log-likelihood function $L(\mathbf{t}|\mathbf{d})$ given in (2) about $\mathbf{t}$, the maximum likelihood (ML) estimator $\hat{\mathbf{t}}$, is calculated as

$$\hat{\mathbf{t}} = \left(\mathbf{A}^T\mathbf{\Lambda}\mathbf{A}\right)^{-1}\mathbf{A}^T\mathbf{\Lambda}\left(\mathbf{y} - \mathbf{b}\right), \tag{4}$$

if and only if $\left(\mathbf{A}^T\mathbf{\Lambda}\mathbf{A}\right)$ is invertible. Since this ML estimator is unbiased, due to $E(\hat{\mathbf{t}}) = \left(\mathbf{A}^T\mathbf{\Lambda}\mathbf{A}\right)^{-1}\mathbf{A}^T\mathbf{\Lambda}\mathbf{A}\mathbf{t} = \mathbf{t}$, and is a function of complete sufficient statistics $T(\mathbf{d})$ of Eq. (3), the estimator $\hat{\mathbf{t}}$ is the minimum variance unbiased (MVU) estimator of $\mathbf{t}$ by Rao-Blackwall-Lehmann-Scheffe theorem [4]. This implies that the estimation error for material decomposition is lower bounded by the corresponding variance, and this is the ultimate performance limit.

Although $\hat{\mathbf{t}}$ of Eq. (4) is the MVU estimator, its variance varies according to $\mathbf{A}$ and $\mathbf{\Lambda}$ determined by energy threshold selection, therefore, we can acquire the optimal energy bin thresholds to minimize the variance of $\hat{\mathbf{t}}$. As our goal is the variance minimization for all materials, the mean squared error(MSE) of $\hat{\mathbf{t}}$ is determined as

$$\text{MSE} = E\left[\|\hat{\mathbf{t}} - \mathbf{t}\|^2\right] = E\left[\text{tr}\{(\hat{\mathbf{t}} - \mathbf{t})(\hat{\mathbf{t}} - \mathbf{t})^T\}\right]$$

$$= \text{tr}\{\text{Cov}(\hat{\mathbf{t}})\} = \text{tr}\{(\mathbf{A}^T\mathbf{\Lambda}\mathbf{A})^{-1}\}. \tag{5}$$

Therefore, the trace of covariance matrix can be used as a metric to minimize in determining the optimal energy levels.

3. DECOMPOSITION ALGORITHM

After selecting the optimal energy level, our goal is to estimate the material compositions. In our statistical framework, the cost function can be now summarized as

$$C(\mathbf{A}, \mathbf{t}, \mathbf{b}) = (\mathbf{y} - \mathbf{A}\mathbf{t} - \mathbf{b})^T\mathbf{\Lambda}(\mathbf{y} - \mathbf{A}\mathbf{t} - \mathbf{b})\,, \tag{6}$$

and we need to minimize $C(\mathbf{A}, \mathbf{t}, \mathbf{b})$ with respect to $\mathbf{A}$, $\mathbf{t}$, and $\mathbf{b}$. Since this problem is highly non-convex optimization, we introduce a calibration block with known length $\{\mathbf{t}_b\}_{b=1}^{B}$. Moreover, in practice, the attenuation coefficient can be different from numerically calculated values over for known spectrum. This is because the detector response function, pulse pileup, etc, can change the measurement attenuation value. Hence, we first need to compensate for those, so we employed the calibration block with known length and estimate the coefficients. Then, the cost function for calibration block becomes

$$\tilde{C}(\mathbf{A}, \mathbf{b}) = \sum_{b=1}^{B}(\mathbf{y}_b - \mathbf{A}\mathbf{t}_b - \mathbf{b})^T\mathbf{\Lambda}_b(\mathbf{y}_b - \mathbf{A}\mathbf{t}_b - \mathbf{b})\,, \tag{7}$$

where $\mathbf{y}_b$ denotes the b-th calibration phantom sinogram measurement and $\mathbf{\Lambda}_b$ is a diagonal matrix composed by measurement $d_{b,i}$ in intensity domain.

3.1. Attenuation coefficient estimation using calibration blocks

Now, the attenuation coefficient matrix is estimated by minimizing the cost function (7) with respect to $\mathbf{A}$ and $\mathbf{b}$. Since the optimization problem is quadratic with respect to $\mathbf{A}$ and $\mathbf{b}$, we can apply successive optimization. By computing the derivatives of Eq. (7) for $\mathbf{a}_k$ and $\mathbf{b}$ and set to zeros, we can obtain $(K+1)$ linear equations of the optimal attenuation coefficient columns $\hat{\mathbf{a}}_k$ and $\hat{\mathbf{b}}$ for $k = 1,\ 2,\ \ldots,\ K$ such that

$$\sum_{l=1}^{K}\left(\sum_{b=1}^{B}\mathbf{\Lambda}_b t_{b,l}t_{b,k}\right)\hat{\mathbf{a}}_l + \left(\sum_{b=1}^{B}\mathbf{\Lambda}_b t_{b,k}\right)\hat{\mathbf{b}} = \sum_{b=1}^{B}\mathbf{\Lambda}_b\mathbf{y}_b t_{b,k},$$

$$\sum_{l=1}^{K}\left(\sum_{b=1}^{B}\mathbf{\Lambda}_b t_{b,l}\right)\hat{\mathbf{a}}_l + \left(\sum_{b=1}^{B}\mathbf{\Lambda}_b\right)\hat{\mathbf{b}} = \sum_{b=1}^{B}\mathbf{\Lambda}_b\mathbf{y}_b. \tag{8}$$

Eqs. (8) can be rearranged in form of $\mathbf{M}\mathbf{x} = \mathbf{Z}$ where $\mathbf{M}$ and $\mathbf{Z}$ are block-wise matrices, and $\mathbf{x}$ is vectorized optimal attenuation coefficients, $\mathbf{x} = [\hat{\mathbf{a}}_1^T,\ \ldots,\ \hat{\mathbf{a}}_K^T,\ \hat{\mathbf{b}}^T]^T$. Therefore, the optimal columns of $\mathbf{A}$ and $\mathbf{b}$ can be estimated by rearrangement of $\mathbf{M}^{-1}\mathbf{Z}$. Figure 1 shows the estimation of attenuation coefficient matrix using calibration block measurements. As shown in the graphs, after attenuation coefficient estimation the intensity values for the measurement are accurately reproduced.

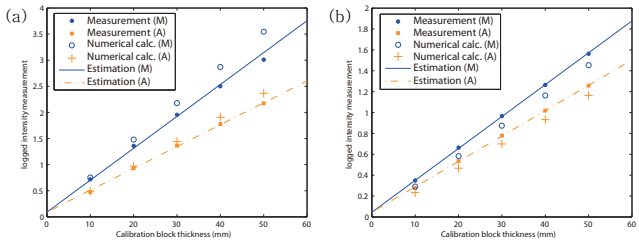


Fig. 1: The sinogram domain measurements of calibration blocks, numerically calculated values, and estimated attenuation coefficients at energy bin of (a) 10-25 keV and (b) 34-49 keV. In text box, (M) represents muscle and (A) represents adipose.

3.2. Material decomposition algorithm

Based on the measurement model, we develop an iterative material decomposition algorithm. If the total thickness of target object is T, the thickness of K-th material can be expressed using the thicknesses of other materials as $t_K = T - \sum_{k=1}^{K-1} t_k$. Based on this, the MVU estimator of $\tilde{\mathbf{t}} = [t_1, \ \ldots, \ t_{K-1}]^T$ can be redefined for $K-1$ bases materials as

$$\hat{\tilde{\mathbf{t}}} = \left(\tilde{\mathbf{A}}^T \mathbf{\Lambda} \tilde{\mathbf{A}}\right)^{-1} \tilde{\mathbf{A}}^T \mathbf{\Lambda} \left(\tilde{\mathbf{y}} - \mathbf{b}\right) \tag{9}$$

where $\tilde{\mathbf{y}} = \mathbf{y} - \mathbf{a}_K T$, and matrix $\tilde{\mathbf{A}}$ is composed of modified attenuation coefficients $\tilde{\mathbf{a}}_k = \mathbf{a}_k - \mathbf{a}_K$. However, the main technical difficult in directly calculating (9) is very large condition number of $(\tilde{\mathbf{A}}^T \mathbf{\Lambda} \tilde{\mathbf{A}})$.

To accelerate the convergence, the following initialization can be used. To improve the decomposition accuracy of bases materials, we assume that the decomposed images are sparse in each material basis and distinguish the images corresponding to each material one by one using matching pursuit (MP) that recursively finds the dominant bases of signal correlating with the residuals from the previous iteration in greedy fashion [5] as shown in figure 2.

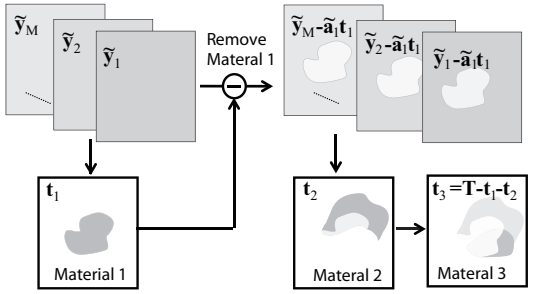


Fig. 2: Scheme of initial material decomposition algorithm using matching pursuit.

Then, based on the statistical model Eq. (2), the optimization problem for best $\mathbf{t}$ is given as

$$\min_{\mathbf{t} \geq 0} (\mathbf{y} - \mathbf{A}\mathbf{t} - \mathbf{b})^T \mathbf{\Lambda} (\mathbf{y} - \mathbf{A}\mathbf{t} - \mathbf{b}) \ , \tag{10}$$

where attenuation coefficients $\mathbf{A}$ and offset $\mathbf{b}$ are estimated by Eq. (7). Since thickness $\mathbf{t}$ is nonnegative value, iterative coordinate descent (ICD) algorithm with positive constraint is applied for estimation of t_k [6]. More specifically, at $(n+1)$-th iteration, the thickness of k-th material is

$$\begin{aligned} t_k^{(n+1)} &= \min_{t \geq 0} \sum_{m=1}^{M} \left(e_m^{(n)} - a_{mk}(t - t_k^{(n)})\right)^2 d_m \\ &= \begin{cases} t_k^{(n)} + \dfrac{\theta_1}{\theta_2}, & t_k^{(n)} \geq -\dfrac{\theta_1}{\theta_2}; \\ 0, & \text{otherwise} \end{cases} \end{aligned}$$

where $\theta_1 = \sum_{m=1}^{M} d_m e_m^{(n)} a_{mk}$, $\theta_2 = \sum_{m=1}^{M} d_m a_{mk}^2$ and $e_m^{(n)} = y_m - \mathbf{A}^m \mathbf{t}^{(n)} - b_m$ with $\mathbf{A}^m$ referring the m-th row of $\mathbf{A}$.

Note that the optimization problem (10) is convex, so any optimization algorithm may converge to a global minimizer. However, as mentioned before, $(\mathbf{A}^T \mathbf{\Lambda} \mathbf{A})$ has very large condition number due to the similar attenuation curves between tissue types. Hence, the convergence rate is very different to the choice of initialization as well as optimization algorithm. In particular, for ICD type algorithm, a good initial guess can accelerate the convergence speed significantly for this type of ill-pose inverse problem.

4. EXPERIMENTAL RESULTS

4.1. System environment

To validate our proposed algorithm, physical breast phantom is used as well as *ex vivo* specimen. For real experiments, we used customized energy resolving PCXD manufactured by DxRay, Inc.(Northridge, CA). The detector is composed of 4 line detector blocks, with 256 Si pixel detectors each. The detector pixel has $100\mu m \times 100\mu m$ resolution, and 5.75 mm thickness. For x-ray generation, tungsten tube is used with 49 kVp and 20 mA. The x-ray tube inherently include Be 0.7 mm filter, and we added Ag 0.03 mm filter. For physical phantom and *ex vivo* specimen, we applied 400 ms exposure while length-known calibration blocks are exposed for 50 ms. This is because the values of calibration blocks can be averaged across the block to increase signal to noise ratio (SNR). For calibration, 15 homogeneous blocks of three materials are used with 5 thickness blocks for each material, from 10 mm to 50 mm with 10 mm increment.

Breast equivalent materials manufactured by CIRS, Inc.(Norfolk, Va) are used for physical phantom as well as calibration blocks. The physical breast phantom is composed of 50% glandular and 50% adipose tissues with arbitrary pattern, and includes 1cm thickness muscle and carcinoma tissue blocks. The shape and locations of inserted blocks are known as figure 3. The measured *ex vivo* breast specimens are acquired after total mastectomy without any chemical processing. The specimen has been compressed into 5 cm thickness. After our multi-energy system measurement, the specimen is moved to dual source x-ray mammography, GE Senographe DS, and a doctor marked malignant region based on the contrast and its morphological characteristics.

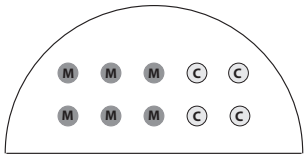


Fig. 3: Malignant tissue inserted slab: (M) refers muscle and (C) refers carcinoma blocks.

4.2. Energy level optimization result

We fixed the minimum bound as 10 keV to avoid the dark current which exists up to 6 keV. The optimal energy level, listed in Table 1, is acquired by minimization of numerically computed $\text{tr}\{(\mathbf{A}^T \mathbf{\Lambda} \mathbf{A})^{-1}\}$ for all possible energy bin combinations. Theoretical optimal energy level was [10-23, 23-35, 35-49]keV. However, due to the system limitation, 23 keV and 35 keV are difficult to be used as thresholds, so we used the nearest energy threshold as [10-25, 25-34, 34-49]keV as optimal energy. As shown in Table 2, the trace of the alternative choice with respect to the theoretical optimal was nearly equivalent, whereas the trace value of arbitrarily selected energy bin was 5 times larger. Material decompositions using optimized energy level and arbitrarily selected energy bin thresholds are compared in figure 4 for the tissue decomposition of 3cm physical phantom after 20 iterations. Both of muscle and carcinoma blocks are accurately decomposed into muscle bases that represents malignant tissue. However, in arbitrarily chosen energy level, [10-30, 30-40, 40-49]keV, malignant tissue image has more background noise compared to the optimal energy measurement decomposition, as pointed out by arrows in magnified view of malignant tissue image. These results confirm that the proposed energy optimization method is indeed practical.

Table 1: Optimized energy bin thresholds for decomposition of carcinoma, glandular and adipose.

X-ray tube filter	Be 0.7mm & Ag 0.03mm			
Object thickness	Energy thresholds (keV)			
3 cm	10	23	35	49
5 cm	10	25	35	49

Table 2: Trace of covariance matrices for each energy level selection: theoretically (th) optimal, experimentally (exp) optimal and non-optimal energy.

	Energy thresholds (keV)				$\mathrm{tr}\{(\mathbf{A}^T\mathbf{\Lambda}\mathbf{A})^{-1}\}$	Ratio
optimal (th)	10	23	35	49	1.3573×10^6	1
optimal (exp)	10	25	34	49	1.5043×10^6	1.1083
non-optimal	10	30	40	49	7.2246×10^6	5.3228

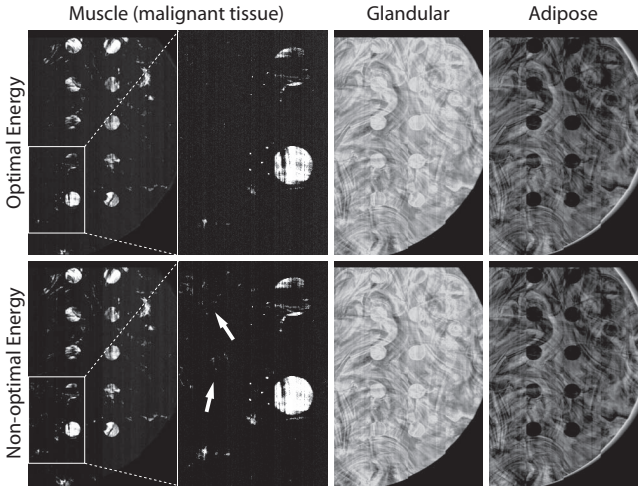


Fig. 4: Material decomposition of 3 cm physical phantom using (top) optimal energy level and (bottom) non-optimal energy level. Malignant tissue images, decomposed into muscle bases, are shown in 0-5 mm scale while other images are shown in 0-35 mm scale.

4.3. Material decomposition result of *ex vivo* data

For 5 cm specimen, we also used [10-25, 25-34, 34-49]keV energy levels. The measurements are decomposed into muscle(malignant tissue), breast tissue, and adipose, and results are acquired after 20 iterations of ICD. The malignant tissue region of *ex vivo* specimen is also accurately decomposed into muscle bases, as shown in figure 5 (c) which is very similar to the doctor marked region in figure 5 (a). Although the adipose region is similarly decomposed in conventional method suggested by Laidevant et al. [1], our algorithm can have better decomposition of malignant tissue and breast tissues. For example, in figure 6, parts of normal tissue regions decomposed as malignant tissues are pointed in white arrows in existing method. This inaccuracy may be due to overestimation caused by small number of calibration blocks.

5. CONCLUSION

A material decomposition algorithm and energy optimization algorithm for PCXD have been proposed under statistical framework. The proposed algorithm successively decomposed malignant tissue from PCXD measurements in both physical phantom and *ex vivo* data acquired in the optimally selected energy bins.

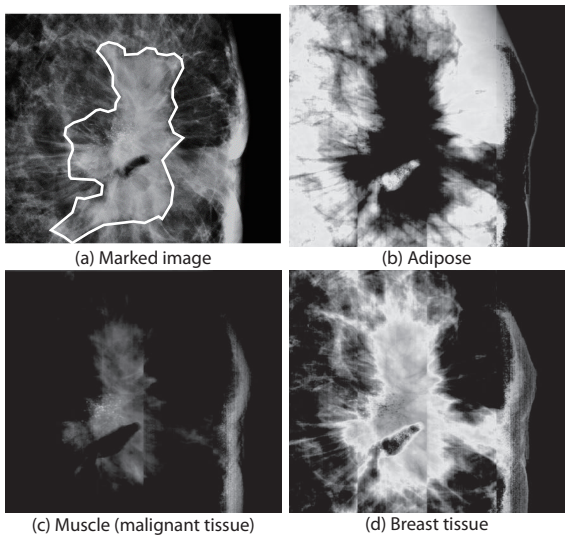


Fig. 5: Material decomposition results of *ex vivo* specimen using proposed method. Images are shown in 0-55 mm scale.

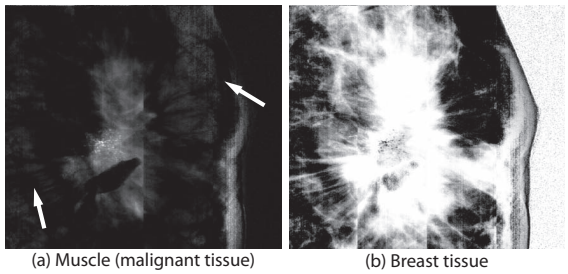


Fig. 6: Material decomposition results using Laidevant method.

6. REFERENCES

[1] A.D. Laidevant, S. Malkov, C.I. Flowers, K. Kerlikowske, and J.A. Shepherd, "Compositional breast imaging using a dual-energy mammography protocol," *Medical Physics*, vol. 37, pp. 164–174, January 2010.

[2] S.C. Kappadath and C.C. Shaw, "Dual-energy digital mammography: Calibration and inverse-mapping techniques to estimate calcification thickness and glandular-tissue ratio," *Medical Physics*, vol. 30, pp. 1110, 2003.

[3] J.L. Ducote and S. Molloi, "Quantification of breast density with dual energy mammography: An experimental feasibility study," *Medical Physics*, vol. 37, pp. 793, 2010.

[4] George Casella and Roger L. Berger, *Statistical Inference*, Duxbury, 2001.

[5] S. G. Mallat and Z. Zhang, "Matching pursuits with time-frequency dictionaries," *IEEE Trans. on Signal Processing*, vol. 41, no. 12, pp. 3397–3415, Dec. 1993.

[6] K. Sauer and C. A. Bouman, "A local update strategy for iterative reconstruction from projections," *IEEE Trans. on Signal Processing*, vol. 41, no. 2, February 1993.